3D-printed poly(oxymethylene): Improving printability via PMMA sacrificial substrates and characterization of the mechanical and thermal properties

Emanuele A. Slejko[1,a], Stefano Seriani[1], Vanni Lughi[1]

[1] *Department of Engineering and Architecture, University of Trieste, Via Alfonso Valerio 6/1, 34127 Trieste, Italy*
[a] Address all correspondence to this author. e-mail: easlejko@units.it

Received: 9 August 2021; accepted: 29 November 2021; published online: 6 January 2022

The fabrication of poly(oxymethylene) by means of additive manufacturing is still a problematic procedure due to the low adhesion with standard printing plates and extended warping. The use of polymers as alternative substrates is an effective way, especially if their glass-transition temperature is below the processing temperatures. Using poly(methyl methacrylate) sheets as sacrificial substrate, standard samples of poly(oxymethylene) are successfully printed, a result achieved in the past only by means of expensive and complex equipment. Furthermore, the mechanical and thermal properties of poly(oxymethylene) upon UV aging up to 500 h are investigated. Our results demonstrate that aging of 3D-printed poly(oxymethylene) causes chain scission and weakening of intermolecular bonds, crystallization of part of the amorphous areas, and results in the embrittlement of the material. The intermolecular structure of poly(oxymethylene) has been investigated by means of Fourier transform infrared spectroscopy.

Introduction

3D printing, or additive manufacturing (AM), is a fabrication technique consisting in the sequential deposition of layers of material to produce a final three-dimensional object. It presents ground-breaking potential for the manufacturing of components with arbitrarily complex geometries in a fast and affordable way, especially when the required production volume is limited. 3D printing has already been applied in several research and industrial fields and its pool of materials and range of applications is constantly expanding [1, 2]. Novel applications are emerging thanks to the development of more efficient printing methods, associated to the expiry of previously unexploited patents and the reduction of the cost of the 3D printers [3]. Rapid and cost-effective fabrication processes, resulting in accessible prototyping capabilities, have so far been the primary driver for the adoption of AM techniques. However, thanks to the improving effectiveness of the process and the increasing reliability of the components fabricated by 3D printing, its use has been recently extended to the production of final products, especially the ones requiring customization at low cost, which represents one of the main limitations of standard mass production techniques. AM utilizes 3D model data as input parameters for the subsequent processing, which can be based on a variety of methods—the choice of which depends on the required material, geometry, part size, performance, and surface finishing. Selective Laser Sintering, Fused Deposition Modeling (FDM), Stereolithography, and Inkjet Printing are currently among the most common techniques [1, 4]. The large consensus gained by 3D printing is mostly due to the advantages in the fabrication of complex geometries with a high degree of precision, leading to the possibility of extensive personal customization and, thanks to the intrinsic additive character of the technique, to a reduction of waste. AM can be applied to a wide range of materials, including metals, ceramics, polymers, and concrete. However, the set of candidates for each material family is still rather limited. Furthermore, each material class relies upon different 3D-printing methods; for example, the most common technique for polymers is FDM. This method is based on the continuous extrusion of a hot plastic filament, which is deposited on a platform or on top of previously printed layers. Thermoplastic behavior is a fundamental feature for FDM 3D printing, as the material must be able to re-solidify properly after melting at high temperature.

Mechanical properties are strongly affected by the thickness of the deposited layers, by the deposition rate, and by the filament orientation, as well as by air gaps within the structure [5, 6]. Even if the thermoplastic material class is quite populated, only less than 50 candidates are available for 3D printing. Quite often, pure polymer products are used as mockups and conceptual prototypes as they lack sufficient mechanical properties and functionality [1]; fiber-reinforced composites and novel materials are under development, currently facing several processing challenges. Nevertheless, they are expected to broaden the field of applicability of AM in the near future. On the other hand, novel high-performance polymeric matrixes are under investigation for their utilization with AM. Many of the most high-performance polymers currently available for FDM 3D printing require printing equipment, which are not economically accessible to the general public. For example, highly performing materials such as Polyetherimide (PEI), also known by its commercial name ULTEM, and polyphenylsulfone (PPSF) require expensive machines characterized by a thermally controlled printing chamber [7]. Indeed, the thermal deformation, i.e., warping, induced by the printing process gradients present in non-enclosed machines, generally prevents successful printing of these high-performance materials [8]. Being able to print similar compounds with low-end desktop 3D printers would benefit the industry and research institutions with considerable cost reductions. Several studies have addressed the topic of optimal adhesion between polymers and standard substrates in FDM, but investigations on alternative substrates are still under development with some notable applications [9–12].

Poly(oxymethylene) (POM) is an engineering thermoplastic material that is driving increasing interest due to its excellent mechanical properties and dimensional stability, and it is primarily employed in the automotive industry. It has one of the simplest chemical structures among polymers, consisting of a backbone of repeating C–O bonds (Fig. 1a and b). It presents a helicoidal structure, and the polar group in the main chain leads to a high melting temperature (170–180 °C) compared to similar plastics. POM presents excellent mechanical properties such as rigidity, toughness, and tensile strength even at temperatures above 100 °C; furthermore, it is resistant to most chemicals and organic solvents. Thermal degradation occurs at high temperatures, and total combustion of the material is favored by its high content of oxygen atoms. POM is primarily used to manufacture engineering components and precision parts like gear wheels, eyeglass frames, bearings, and fasteners, mainly because its low surface friction and dimensional stability. Despite the aforementioned advantages, POM is currently not available on the market as parts on demands, and it is rarely supplied as 3D-printing filament. In fact, it is not easy to 3D-print POM with consistent and reliable results, mostly for two different reasons. The first one is related to the

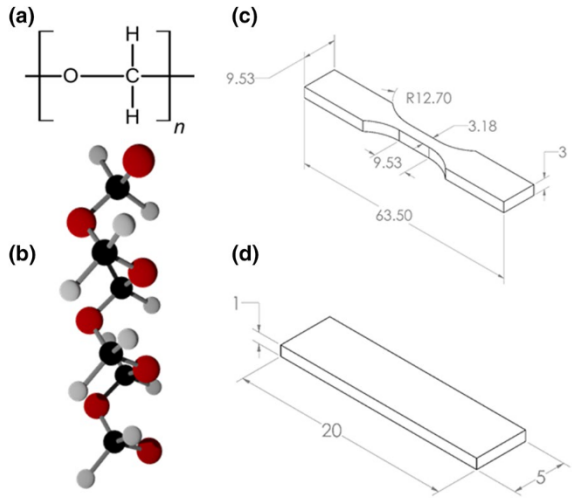

Figure 1: (a) Chemical formula of poly(oxymethylene) and (b) schematic molecular structure for a single chain. (c) The 3D model of the mechanical testing ASTM D638-03 type V dogbone sample and (d) the adhesion campaign sample for evaluation of the adhesion over different substrates. Dimensions are in mm.

self-lubricating behavior of POM, which hinders the adhesion of the first deposited layer of material on the printing bed. The second reason is related to the thermal shrinkage of the material, which causes extended dimensional changes during inhomogeneous cooling. At the current stage, printing glues and ABS juice, as examples, are common choices to promote adhesion between the printing plate and the first layers, while the dimensional change can be mitigated only by using a heated chamber and appropriate printing bed temperatures. These issues are the subject of current investigations, as they strongly limit the applicability of poly(oxymethylene) as material for FDM [13–15], thus, sensibly reducing the impact that this material can have on innovative technological applications based on AM.

In this contribution, we analyze the mechanical and thermal properties of 3D-printed POM samples after aging under UV radiation and compare the mechanical response with that of the bulk material manufactured by traditional techniques. The mechanical and thermal properties, as well as the aging behavior, have already been investigated for conventionally produced POM; however, at the best of our knowledge, our contribution is the first to address these topics for 3D-printed POM. In general, investigation of the properties of 3D-printed materials represents a critical point in the adoption of AM by the industry, as there is still a lack of knowledge and of reliable simulation models for predicting the functional and structural behavior of 3D-printed parts, limiting the applicability of AM and the extension of its available materials pool. Furthermore, to obtain reliable and repeatable printed objects, we propose a simple and effective way to promote adhesion

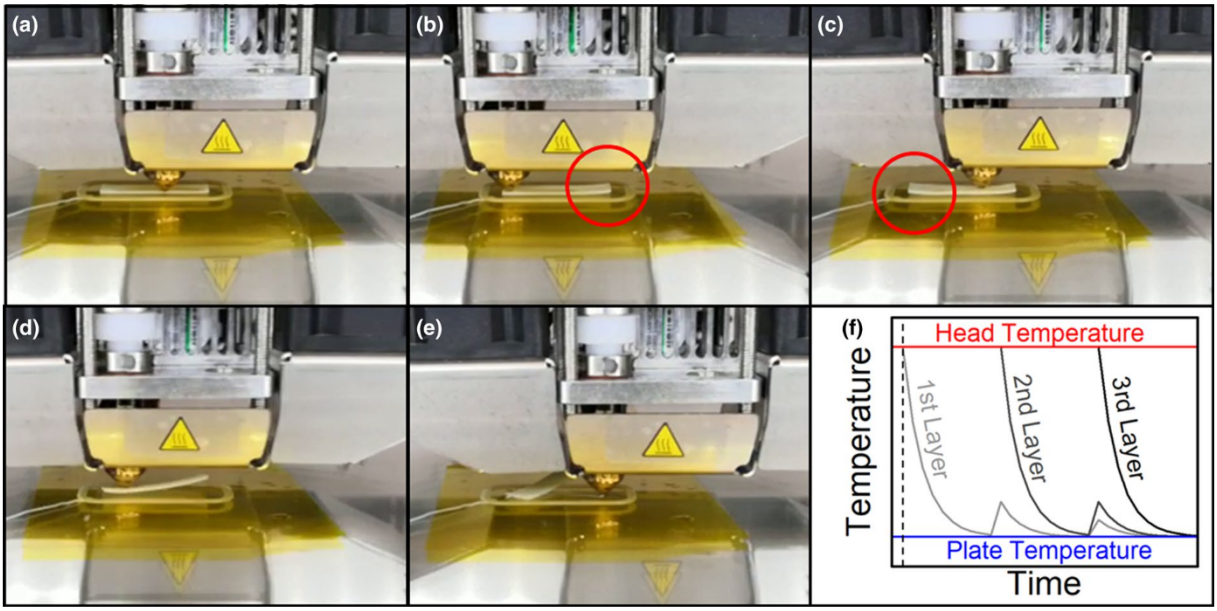

Figure 2: (a–e) Successive snapshots of the printing process on PI film. Red circles in (b) and (c) indicate the first detachment spots on the edge of the geometry. (f) Scheme of the temperature profile for the first 3 layers as a function of time. Horizontal lines represent the printing head temperature (red) and the printing plate temperature (blue). After extrusion from the printing head, the material cools down and stabilizes at the bed temperature. Upon deposition of a new layer, a small temperature spike on the previous deposited layers is expected. Dashed vertical line indicates the beginning of the printing process. Comparing different layers, a temperature gradient is always present and it is responsible of the distortion during the cooling of the layers.

between the printing base and the extruded material recurring to poly(methyl methacrylate) (PMMA) as sacrificial substrate. The production of 3D-printed POM parts is a hot topic for the aerospace sector, where AM is obtaining ever-growing attention for its potential to develop innovative production systems for in-orbit manufacturing and for cost-effective Small Satellite solutions [16, 17]. From this perspective, the characterization of polymers (and specifically of POM) upon aging is particularly important as in space applications the atmospheric shield that masks the incoming sunlight radiation is absent or limited. Being able to print POM by AM in a reliable way and understanding the physical and chemical aspects during its use is still an open research topic that can contribute substantially to the future development of AM in several industrial sectors. In addition, the ability to print without having to resort to expensive machines with thermostatic chambers would enable the use of this material to a wider community thanks to a considerable cost reduction of the production process.

Results and discussion

Improved printability of POM by FDM

In conventional FDM instrumentation, the heating plate is usually made of glass, which allows good wettability thanks to its high surface energy, and long-term durability thanks its chemical stability. Other reasons for the choice of glass are that it is easily cleaned and that the production of flat, smooth, and thermally stable surfaces is cost effective. In our specific case, the drawback is that POM does not establish strong bonds with glass and, as soon as the deposition starts, the two materials detach due to warping. In order to investigate strategies to improve the performance of 3D-printing POM, we performed a set of experiments that involved the printing of the simple geometry shown in Fig. 1d. Bare glass, PI tape (commercial Kapton®), and PMMA sheets were used as substrates. PI tape has been selected as it represents a common alternative to glass when adhesion is critical. On glass, detachment occurred immediately upon printing of the very first layers. The polyimide tape showed a positive effect on the adhesion; however, detachment occurred anyway after deposition of a small number of layers, and the mode of failure was similar to that observed on the bare glass. The detachment typically starts from the border of the printed part (see red circles in Fig. 2b and c) and extends over the entire contact area after a few tenths of a second, up to the point of complete detachment (Fig. 2d and e)—leading to the failure of the printing. The deformation is mainly caused by differential shrinkage due to the thermal gradient among printed layers [18, 19]. As schematically illustrated in Fig. 2f, each layer of the printed part has a different temperature; the differential cooling results in the build-up of residual stresses, which can ultimately overcome the adhesion

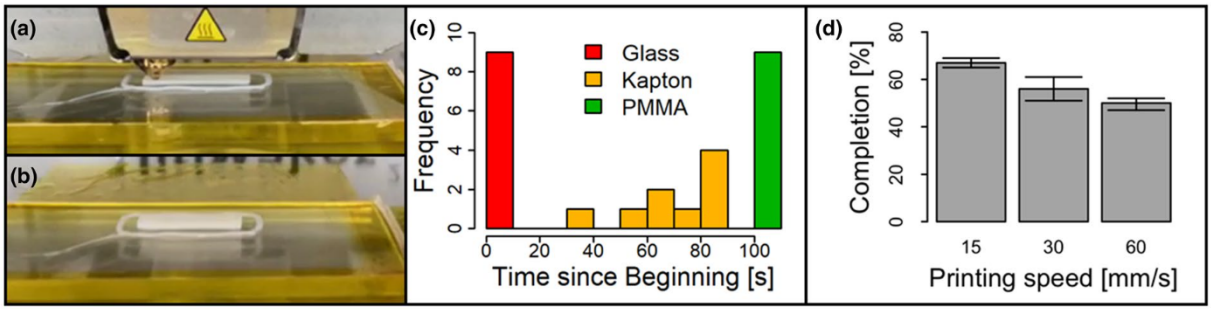

Figure 3: (a) printing process on PMMA and (b) its completion. (c) Distribution of the attachment time as a function of the contact material: bare glass fails immediately, Kapton® has an average time of 70 s before detachment, PMMA guarantees completion of the printing (110 s). (d) Completion percentage as a function of the printing speed for samples on Kapton® tape.

forces, leading to detachment and subsequent warping of the object and failure of the process [18].

Using PMMA sheets as substrates on top of the printing bed, instead, considerably improved the performance of the process, allowing completion of the printing (Fig. 3a and b).

For a quantitative evaluation of these observations, nine printing experiments have been conducted for each of the substrates (glass, PI, and PMMA), recording the time required to complete detachment. In case no detachment occurred during printing, the recorded time was that of the completed print process itself. The results are presented in Fig. 3c. The best adhesion, as already mentioned, occurred with PMMA, which in our experiment was the only substrate to guarantee completion of the printing (110 s, on average, to finalize the geometry). For the other two materials, detachment took place immediately for bare glass, or after a short time for PI tape. For the latter, the average time to detachment was 70 s, with a rather broad dispersion (yellow bars in Fig. 3c). The influence of the printing speed is illustrated in Fig. 3d: reducing the speed has a beneficial effect for samples printed on PI tape as the percentage of completion, evaluated as the ratio between the time for detachment and the time to successfully complete the printing, increases. Even if there is an improvement, the percentage is still far from 100%. Instead, PMMA substrate guarantees completion of the printing, irrespective of the investigated printing speed.

A schematic representation of the distribution of temperature and stresses along the printed part is illustrated in Fig. 4a: while the fused filament is deposited on top of the object, previous layers have already cooled down and a thermal gradient arises within the structure. This causes the presence of in-plane shear stresses within the printed part, which eventually result in deformations [18]. As the glass-transition temperature for Kapton® is in the range of 360–410 °C, no softening can occur for the Kapton® substrate at the deposition temperature—and even more so for glass. Therefore, neither glass or PI can accommodate the thermally induced distortions (Fig. 4b and c) by deforming themselves [20, 21]; for these two materials, a

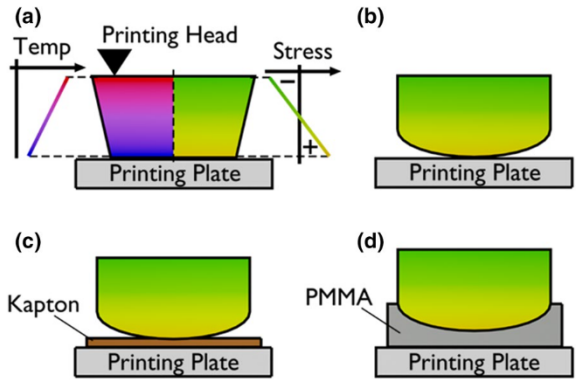

Figure 4: (a) Thermal and stress distribution along the height of the printed object for the first deposited layers. The first layer has already cooled down, while the top layer has a higher temperature. This results in a shear stress applied to the material, generating the warping of the structure. (b) Part printed on bare glass. The negative effect of warping is not reduced by any deformation of the plate and, thus, the contact area between part and substrate is sensibly diminished during printing. (c) Part printed on PI tape. Since PI is well below its glass-transition temperature, no deformation can occur and again the contact area is reduced during printing. (d) Part printed on PMMA sheet. PMMA can plastically deform and accommodate a portion of the warping, maintaining an extended contact area between the substrate and the printed part.

reduction of the contact area occurs up to the point of complete detachment. The same effect is reported for thick POM samples printed on PMMA: as the volume of the part increases, thermal distortions add up. We have observed partial detachment while printing sample of 5 mm or 10 mm thickness, indicating that other solutions (like the use of a heating chamber, for example) have to be applied to produce high-quality parts.

The improved printability with PMMA is related to the fact that, since the printing material is deposited at high temperature (240 °C) and the printing bed is kept at 100 °C, the PMMA substrate is very close to its glass-transition temperature T_g (105 °C for atactic PMMA), resulting in an increased rubber-like behavior of the substrate [22] and, therefore, a rather high deformability [23–25]. Deformation of the substrate accommodates

TABLE 1: Bulk properties of POM copolymer material, as found in Granta® CES Selector database, compared to 3D-printed samples developed in this study, respectively, without aging, after 100 h aging, after 500 h aging, and at 60 °C.

Mechanical property	Conventional POM	POM 0 h	POM 100 h	POM 500 h	POM HT
Young's modulus (GPa)	2.9	1.6 (±0.1)	1.7 (±0.1)	1.7 (±0.1)	1.1 (±0.1)
Tensile strength (MPa)	69.0	55.1 (±1.2)	54.4 (±1.1)	54.6 (±1.0)	40.9 (±3.4)
Elongation at break (%)	54.8	22.6 (±3.1)	19.2 (±1.0)	14.4 (±0.6)	21.9 (±1.8)

In parenthesis, the standard deviation related to each measurement.

the warping tendency of the printed part, partially relaxing the stresses generated by the thermal gradient, simultaneously maintaining extended contact area, as schematically indicated in Fig. 4d. From a different perspective, a portion of the strain energy is dissipated by the plastic deformation of the substrate. The fact that a shallow impression is left on the substrate after removing the part (Fig. SI1) supports the twofold mechanisms described here.

Furthermore, the adhesion in a polymer–polymer coupling can benefit from the formation of interfacial interactions, such as hydrogen bonding, promoted at high temperature by the small rearrangements of the rubbery network chains [26]. Indeed, this aspect is expected to be enhanced by the processing temperatures, which are close to the glass-transition temperature of PMMA. One further advantage of this solution is that, as soon as the printing process is complete, the temperature drop weakens the adhesion and the printed object is, therefore, easily removed from the substrate, avoiding the common inconvenience of partial welding between the printed part and the bed. While the importance of the glass-transition temperature had previously been considered for improving the adhesion during FDM [15, 27], the printed polymer-printing bed combination (here specifically POM and PMMA) to reach superior adhesion has not been investigated before. It is worth mentioning that, while the warping of the printed part is not avoided, the improved adhesion enables completion of the printing. More investigation is still needed, specifically in terms of the printed part geometry and extension, especially for what concerns the ratio between contact area and volume, since thermal gradients are critical when considering distortions during printing; indeed, cooling rate is strongly correlated to reducing the internal stresses [28]. Nevertheless, our results clearly indicate how the printing bed material can have a great impact on the performance of the process because of the thermomechanical interactions between the part and the substrate. While glass has superior stability and durability, it is seldom the optimal counterpart for the material being printed, as in the case of POM. Implementing polymers as novel single-use sacrificial substrates can improve the effectiveness of FDM additive manufacturing for materials that cannot be 3D printed with the current standard configurations, without recurring to expensive and complex instrumentations.

Thermomechanical properties of 3D-printed POM

The mechanical properties of ASTM dogbone samples have been tested under uniaxial tensile load and flexural load to evaluate the ultimate strength, strain at rupture, and Young modulus of the material. Reference values found in the literature are reported in Table 1 and are considered as a benchmark in our analysis. During our experiments, we have observed that the mechanical properties of printed samples are lower compared to the references; this is expected since it is well known that the additive manufacturing technique negatively affects the final properties of printed parts in most cases [29–31]. Young modulus, tensile stress, and deformation at failure of samples processed with different aging times are reported in Table 2 and Fig. 5a–c.

The Young Modulus E at room temperature has been estimated by 3-point bending test and resulted in 1.6 GPa without any aging treatment; this value is almost half of the bulk elastic modulus of conventionally produced POM, which on average is 2.9 GPa. This difference is mainly due to printing conditions (e.g., intra-layer filament bonding) which strongly affect the mechanical properties [7, 29, 32]. Aging caused a limited increase of elasticity modulus (1.7 GPa) for both 100 h and 500 h aging, probably due to the scission of molecular chains and increase of density of the materials, as reported for organic coatings [33]. This behavior is coherent with the increase of crystallinity we have observed by thermal analysis after aging. The responses to UV aging have been investigated on ultimate stress and strain at rupture too, indicating how POM can sustain radiation without degradation of its strength but sensibly limiting the plastic deformation before rupture. A slight modification of its appearance has been observed, in accordance to typical

TABLE 2: Thermal properties for POM samples at different aging time.

Aging time (h)	Melting temperature (°C)	Enthalpy of fusion (J g^{-1})	Crystallinity (%)
0	169.1	148.1	67.3
100	164.9	160.0	72.7
500	162.9	170.1	77.3

Crystallinity is evaluated considering the standard enthalpy of fusion for POM copolymer, which is 220.0 J g^{-1}.

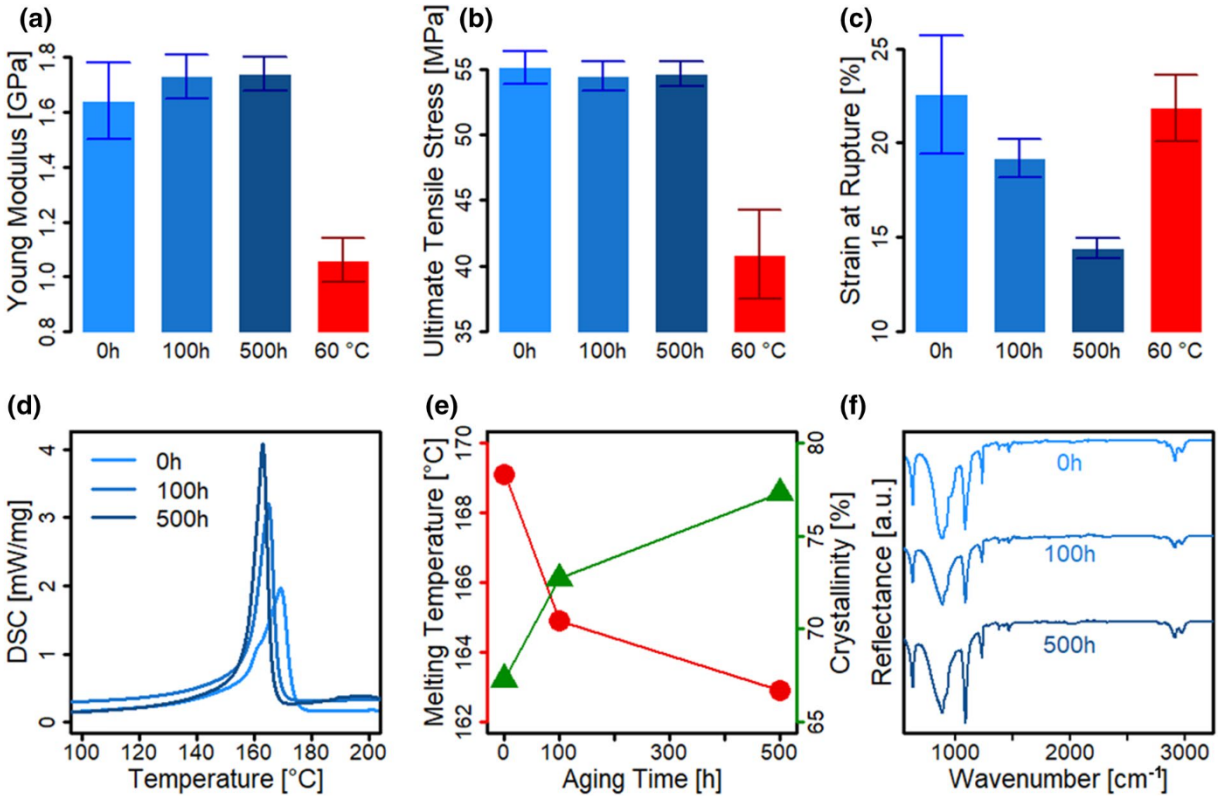

Figure 5: Mechanical properties of POM samples a room temperature (before and after aging) and at 60 °C: (a) Young modulus, (b) tensile stress, (c) strain at rupture. (d) DSC analysis of samples after different aging times. The height of the peak of the curve increases while its position decreases after the aging, indicating a change in the thermal properties of the material, especially the melting temperature and the enthalpy of fusion. (e) Melting temperature and percentage of crystallinity as obtained from DSC traces. Molecular rearrangement during aging causes a reduction of the melting temperature and a concurrent increment in crystallinity. Lines between dots are guides for the eye. (f) FTIR spectra for samples at different aging time. Except the increase of peak at 1093 cm^{-1}, no other major differences are detected.

discoloration due to high-temperature deterioration, as reported in the literature for the bulk material [34]. No sensible reduction of the ultimate strength was detected upon aging treatment: the observed values were roughly 14% lower than the reference for conventional POM. The most substantial reduction is reported for the elongation at break, where the experimental results indicate a decrease of almost 40%. These results are consistent with the reduction of ductility reported in the literature [35, 36], where degradation of POM by oxidation caused the embrittlement of the material. During aging, two different responses are possible: chain scission or crosslinking. It has been demonstrated that POM incurs in polymer chain scission, resulting in a decrease of the mean molar mass, which leads to embrittlement [36, 37]. As observed for our samples, chain scission affects the plastic deformation of the material, sensibly reducing the strain at rupture, but does not significantly alter the ultimate stress of the polymer [33, 34, 36, 38, 39]. Furthermore, hydrogen bonds between chains are weakened. This, in association with the decline in molecular weight (MW), is expected to lead to a decrease in the mechanical properties, especially the deformation at rupture, as already indicated for other polymers [40].

We performed an analysis of the mass of samples before and after the aging process, but no substantial difference has been observed (results are reported in Fig. SI2). The prolonged permanence at 60 °C under UV radiation exposure did not cause a detectable mass loss, coherently with the induction period observed previously for POM in air and atmospheric pressure [37]. Bending at 60 °C led to an elasticity modulus of 1.1 GPa, well below the values at room temperature, indicating extensive softening of the material (Fig. 5a). The Young modulus dropped to about 62% of the room temperature value when tested at 60 °C, indicating the low resistance to temperature of the material. This behavior is caused by the contraction of the typical helical chain, consisting of a sequence of C-O bonds, of POM: at higher temperature, the conformation is more disordered and a contraction of the chain occurs due to skeletal torsional motion [34, 41]. The marked influence of temperature on POM is also observed in the ultimate tensile stress reduction: the disordered state of molecular chains causes a limited resistance, while no substantial increase in elongation, and thus in ductility, is observed at 60 °C.

Figure 5d shows DSC traces at increasing UV exposure time. As can be seen, aging is associated to an increase of crystallinity in the material, as suggested by the higher enthalpy of fusion of samples after the aging process. This can be due to the event of post-crystallization during aging, as molecules from amorphous regions can rearrange themselves in crystallites with the concurrent reduction of MW and the weakening of bonds between molecules, as discussed before for the mechanical properties [40]. The process of integration into the crystalline phase of polymer segments derived from chain scission in the amorphous phase is known as chemicrystallization [42]. The decline of molecular weight and the introduction of photo-oxidation products are also associated to the reduction of the melting temperature, as indicated in Fig. 5e and Table 2 from DSC analysis. A similar mechanism has been recently observed in laser-sintered polyamide upon degradation via exposure to UV radiation [43]. The value of 169.1 °C, furthermore, indicates that our starting material was a POM copolymer (confirmed by manufacturer's datasheet), as the homopolymer presents a higher melting temperature [34]. The crystallinity of POM is evaluated based on the heat of fusion for 100% crystalline POM copolymer (220.0 J g^{-1}). During aging, an increase of 10% in crystallinity is reported, coherently with our explanation of the degradation at molecular scale of the material (Fig. 5e).

A slight color difference of the sample's surface was observed by visual inspection. To further investigate how the molecular structure of POM changed as result to aging, we recurred to FTIR analysis. No major change has been detected in the spectra (see Fig. 5f). The two absorption bands at 2981 cm^{-1} and 2923 cm^{-1} are attributed to symmetric stretching of CH_2, while the band at 1469 cm^{-1} is assigned to the bending vibration of CH_2 groups. The 1383 cm^{-1} band arises from the wagging of CH_2, while the band at 1236 cm^{-1} is attributed to the CH_2 twisting vibration. The spectra show an intense absorption at 1089 cm^{-1} and 891 cm^{-1} and a weak band at 1136 cm^{-1}: these are attributed to the asymmetric stretching vibration of C–O–C groups. The C–O–C symmetric stretching, instead, appears at 933 cm^{-1}. The absorption band at 630 cm^{-1} is assigned to the O–C–O groups bending vibration [44, 45]. Two crystal forms of POM exist: orthorhombic and hexagonal. While the former is more stable at low temperatures, the latter prevails because of its low rate of conversion [34]. The hexagonal system consists of a 9/5 helical conformation, containing both folded-chain crystals (FCC) and extended-chain crystals (ECC). The FCC and the ECC structures may be clearly distinguished by Fourier Transform Infrared spectroscopy, as this technique is highly sensitive to morphological changes [34, 46]. In our spectra, the strong intensity of the 891 cm^{-1} vibration band indicates a high percentage of the ECC structure (see Fig. SI3). To the best of our knowledge, this represents the first experimental observation of the morphological structure of 3D-printed POM produced by Fused Deposition Modeling. The percentage of ECC structure remains high throughout our investigation, irrespective to aging time. In addition, no major changes of the absorption bands have been detected in the spectra, discarding the hypothesis of an extensive variation in the chemical composition of the material upon aging.

The thermal stability of 3D-printed POM has been evaluated via TGA (Fig. 6). All samples present a residual mass lower than 1.5% at 600 °C, indicating a complete degradation and the absence of inorganic additives inside the material. Furthermore, no major differences have been detected between the pristine filament and the sample after printing, indicating that the printing process does not affect the thermal stability of the material. A sensible reduction of the degradation temperature, instead, is reported upon aging. Specifically, after 500 h aging, the onset temperature for degradation occurs at 265.2 °C and the end temperature is 303.0 °C. For the pristine filament, the onset temperature is 280.5 °C and the end point is 306.1 °C. This behavior indicates an easier degradation of the material upon heating.

Conclusions

In this contribution, we have demonstrated a simple and effective modification of the printing process to improve adhesion of POM with the heating bed and to successfully complete the fabrication of standard samples. The modification is based on the utilization of PMMA, instead of bare glass or PI, as sacrificial substrate. The high temperatures of the printing process guarantee that PMMA is above its glass temperature, enhancing fixation of the printed part on the plate. We have furthermore investigated how 3D-printed POM reacts to different UV aging times in terms of mechanical and thermal properties. While the tensile stress and Young modulus present no variation, there is a marked reduction of the strain at rupture, from 22.6 to 14.4%, mainly related to changes in the molecular weight and molecular arrangement caused by aging. The mechanical properties of 3D-printed samples are lower compared to those of conventional POM, principally due to the nature of the additive manufacturing fabrication process. Furthermore, the Young modulus degrades sensibly at 60 °C, denoting the low resistance of the material to high temperatures. Thermal analysis indicates an increment in crystallinity on the 3D-printed samples, from 67.3 to 77.3%, coherently with the observed behavior during mechanical tests, while IR spectroscopy shows no major changes in the chemical composition after aging. Our observations indicate that, upon increasing aging time, 3D-printed POM undergoes the same molecular rearrangements as conventionally fabricated POM, with an increase in crystallinity and a consequent reduction of strain at rupture. The embrittlement of the material

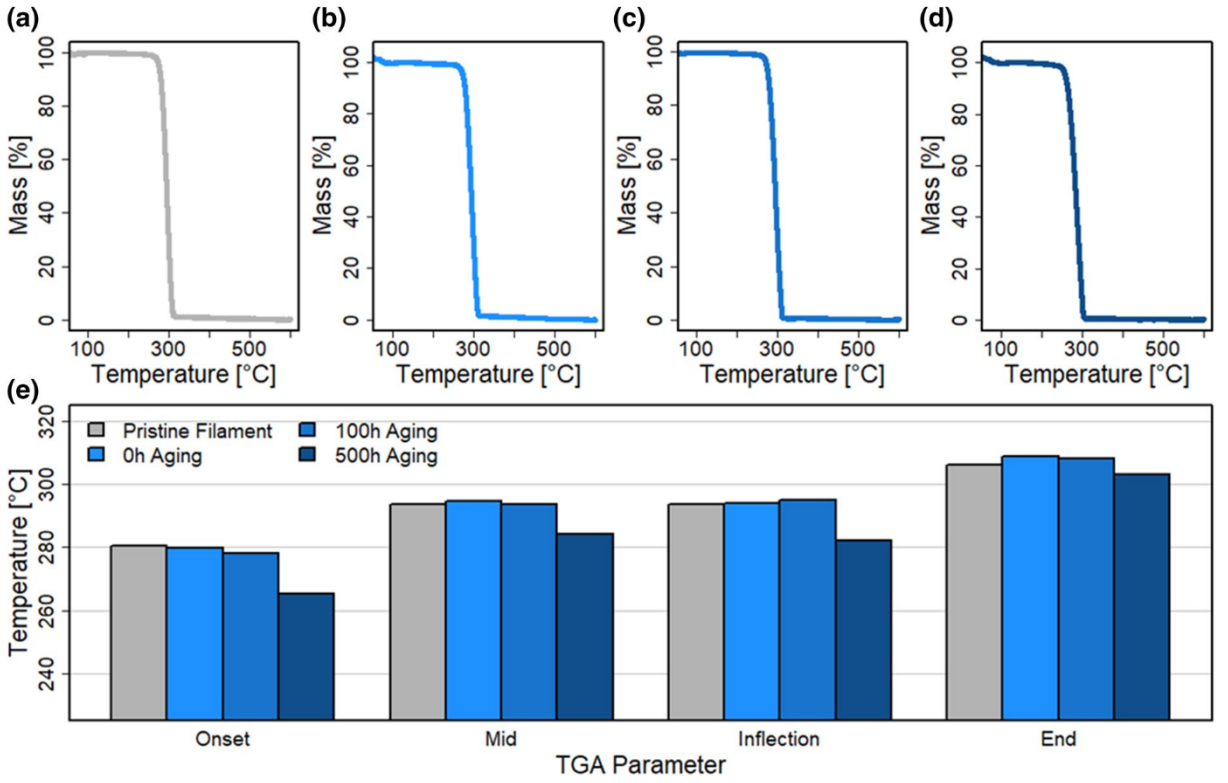

Figure 6: Thermogravimetric analysis of 3D-printed POM samples. Mass change upon heating of (a) pristine filament, (b) 3D-printed POM without aging, (c) 3D-printed POM with 100 h aging, and (d) 3D-printed POM after 500 h aging. (e) Temperatures for the onset, mid-point (50%), inflection, and end point of the thermal degradation.

is related to the scission of molecular chains and weakening of intermolecular bonds, resulting in the degradation of molecular weight distribution and triggering the rearrangement of amorphous areas into new crystallites. Finally, the intermolecular structure of 3D-printed POM has been studied for the first time, indicating a large portion of ECC configuration in the hexagonal phase, as already observed for the conventionally fabricated polymer. All these results are expected to be helpful for laying the basis for the industrial processing of POM by means of additive manufacturing.

Material and methods

POM filament

The filament used in this research has been provided by Capifil under the trademark of Actifil 3D. It is worth noting that at the time of preparation of this manuscript, POM filament is rather difficult to find on the market, and even the most established suppliers of 3D-printing raw materials do not offer this product.

Printer, samples geometry, and print settings

The mechanical testing dogbone sample geometry is based on the American Society for Testing Materials (ASTM) standard D638-03 type V; the geometry of the samples used for adhesion testing is a simple $20 \times 5 \times 1$ mm slab. The samples, shown in Fig. 1c and d, were designed using the software Dassault Systèmes Solidworks® 2017. The geometry was saved as.stl file and exported to the 3D-printing pre-processor Cura 2.6.0. The main parameters for 3D printing the ASTM samples and for

TABLE 3: Main parameters for the 3D-printing process for ASTM dogbone samples and for adhesion samples.

Parameter	ASTM dog-bone samples	Adhesion samples
Extruder temperature (°C)	240	240
Print bed temperature (°C)	100	100
Layer height (mm)	0.06	0.10
Initial layer height (mm)	0.27	0.27
Wall thickness (mm)	1.05	0.40
Infill density	100%	100%
Infill pattern	Lines	Lines
Print speed (mm s^{-1})	50	50
Initial layer print speed (mm s^{-1})	30	30
Cooling fan	100%	100%
Brim width (mm)	8	0

the adhesion samples are summarized in Table 3. The printer used in this work is an Ultimaker® 2+.

PMMA sacrificial substrates and Kapton® film

As previously mentioned, POM presents weak adhesion to other materials and undergoes a marked thermal distortion during cooling; the combination of these two factors commonly leads to partial or total detachment of the part during printing [13]. We investigated the effect of two different plastic substrates with the aim of overcoming this issue: a 5 mm-thick poly(methyl methacrylate) sheet and a Kapton® film. Both were fixed on top of the glass printing bed. Kapton® was selected as a reference as it is commonly utilized as an alternative material for the printing bed. PMMA was selected for its ability to promote good adherence to many materials and because of its rather low softening temperature; thanks to the latter, the substrate is easily deformed at typical printing temperatures, thus, promoting relaxation of the stress induced by inhomogeneous cooling and hindering detachment of the part from substrate during printing.

Mechanical test equipment

Uniaxial tensile and bending tests have been performed on a Shimadzu AGS-X test machine equipped with a 10 kN load cell. Ultimate strength and elongation at rupture have been evaluated via tensile tests, while the Young modulus has been measured via bending tests [47, 48]. The mechanical properties at 60 °C have also been evaluated by using a heated chamber fitted to the same instrumentation. Dogbone samples have been heated in an oven at 60 °C for 30 min and then placed in the test chamber for 10 min before starting the test. This procedure guarantees thermal equilibrium inside the material and avoid any distortion due to temperature gradients. Three samples for each experiment have been prepared, and tests were conducted according to ASTM D638-03 for the tensile behavior and ASTM D790 for the flexural behavior.

Thermal test equipment

Differential Scanning Calorimetry (DSC) testing has been carried out with a Netzsch DSC 200 F3 Maia instrument to investigate the thermal behavior of the material. 6 mg of material has been collected from 3D-printed samples and heated inside aluminum crucibles from 25 to 210 °C with a rate of 10 °C·min^{-1}. Thermogravimetric analysis (TGA) was performed on samples in order to characterize their thermal stability. 6 mg of material was heated using a Netzsch STA 409 EP instrument from 30 to 600 °C, with a heating rate of 10 °C·min^{-1} in dynamic air.

Aging equipment

Accelerated aging experiments have been performed using a Q-Sun Xenon test chamber Model Xe-1 manufactured by Q-LAB. The chamber is equipped with a xenon-arc lamp emitting radiation in the UV–IR range. The peak wavelength is maintained in the range 340 ± 10 nm. The condioning parameters have been selected according to the standard by International Organization for Standardization (ISO) 4892-part 2. During treatment, the temperature was kept at 60 °C.

Infrared spectroscopy equipment

A Thermo Nicolet Nexus 470 Fourier Transform IR spectrometer equipped with Avatar Diffuse Reflectance accessory has been used for the measurement of FTIR spectra of aged samples. The spectra have been collected in the range 400–4000 cm^{-1}; the nominal resolution of the spectrometer was 2 cm^{-1}.

Acknowledgments

We would like to thank the company Capifil for providing the starting material for this research and Dr. Luca Cozzarini for the help performing the mechanical and thermal characterization of samples. We are grateful to Dr. Lucia Marsich for the TGA measurements.

Author contributions

EAS: Conceptualization, Data Curation, Formal Analysis, Investigation, Visualization, Resources, Writing—original draft, Writing—Review and Editing. SS: Methodology, Formal Analysis, Investigation, Validation, Resources, Writing—Review and Editing. VL: Funding Acquisition, Writing—Review and Editing.

Funding

This research has been funded by the "Higher Education and Development" program (code FP1619892003, channel 1420AFPLO2) by European Social Fund.

Data availability

Not applicable.

Code availability

Not applicable.

Declarations

Conflict of interest The authors declare no competing interests in this research.

Supplementary Information

The online version contains supplementary material available at https://doi.org/10.1557/s43578-021-00455-4.

References

1. T.D. Ngo, A. Kashani, G. Imbalzano, K.T.Q. Nguyen, D. Hui, Additive manufacturing (3D printing): a review of materials, methods, applications and challenges. Composites B **143**, 172–196 (2018). https://doi.org/10.1016/j.compositesb.2018.02.012
2. J.Y. Lee, J. An, C.K. Chua, Fundamentals and applications of 3D printing for novel materials. Appl. Mater. Today. **7**, 120–133 (2017). https://doi.org/10.1016/j.apmt.2017.02.004
3. L.E. Murr, Frontiers of 3D printing/additive manufacturing: from human organs to aircraft fabrication. J. Mater. Sci. Technol. **32**, 987–995 (2016). https://doi.org/10.1016/j.jmst.2016.08.011
4. S.C. Ligon, R. Liska, J. Stampfl, M. Gurr, R. Mülhaupt, Polymers for 3D printing and customized additive manufacturing. Chem. Rev. **117**, 10212–10290 (2017). https://doi.org/10.1021/acs.chemrev.7b00074
5. K.R. Hart, R.M. Dunn, J.M. Sietins, C.M. Hofmeister Mock, M.E. Mackay, E.D. Wetzel, Increased fracture toughness of additively manufactured amorphous thermoplastics via thermal annealing. Polymer **144**, 192–204 (2018). https://doi.org/10.1016/j.polymer.2018.04.024
6. H.J. O'Connor, A.N. Dickson, D.P. Dowling, Evaluation of the mechanical performance of polymer parts fabricated using a production scale multi jet fusion printing process. Addit. Manuf. **22**, 381–387 (2018). https://doi.org/10.1016/j.addma.2018.05.035
7. R.J. Zaldivar, D.B. Witkin, T. McLouth, D.N. Patel, K. Schmitt, J.P. Nokes, Influence of processing and orientation print effects on the mechanical and thermal behavior of 3D-Printed ULTEM ® 9085 Material. Addit. Manuf. **13**, 71–80 (2017). https://doi.org/10.1016/j.addma.2016.11.007
8. T.E. Shelton, Z.A. Willburn, C.R. Hartsfield, G.R. Cobb, J.T. Cerri, R.A. Kemnitz, Effects of thermal process parameters on mechanical interlayer strength for additively manufactured Ultem 9085. Polym. Test. **81**, 106255 (2020). https://doi.org/10.1016/j.polymertesting.2019.106255
9. B. Sun, F. Jiang, D. Yang, M. Li, Y. Ren, Q. Feng, C. Qian, The debonding failure mechanism analysis and performance experiments of 3D printed wiring boards, in *2020 21st Int. Conf. Electron. Packag. Technol. ICEPT 2020*. (2020). https://doi.org/10.1109/ICEPT50128.2020.9202423.
10. F.A. Doronin, I.V. Nagornova, G.O. Rytikov, L.G. Varepo, V.G. Nazarov, The general approach to the 3D-printing process quality estimation on the modified polymer substrates. J. Phys. Conf. Ser. (2020). https://doi.org/10.1088/1742-6596/1546/1/012007
11. F.L. Redondo, M.C. Giaroli, M.A. Villar, A.G.O. de Freitas, A.E. Ciolino, M.D. Ninago, Direct 3D printing of poly(lactic acid) on cotton fibers: characterization of materials and study of adhesion properties of the resulting composites. Macromol. Symp. **394**, 1–7 (2020). https://doi.org/10.1002/masy.201900190
12. F. Kotz, M. Mader, N. Dellen, P. Risch, A. Kick, D. Helmer, B.E. Rapp, Fused deposition modeling of microfluidic chips in polymethylmethacrylate. Micromachines. **11**, 5–8 (2020). https://doi.org/10.3390/mi11090873
13. I. Muro-Fraguas, E. Sainz-García, A. Pernía-Espinoza, F. Alba-Elías, Atmospheric pressure air plasma treatment to improve the 3D printing of polyoxymethylene. Plasma Process. Polym. **16**, 1–14 (2019). https://doi.org/10.1002/ppap.201900020
14. E.M. Liston, L. Martinu, M.R. Wertheimer, Plasma surface modification of polymers for improved adhesion: a critical review. J. Adhes. Sci. Technol. **7**, 1091–1127 (1993). https://doi.org/10.1163/156856193X00600
15. A. Das, C.A. Chatham, J.J. Fallon, C.E. Zawaski, E.L. Gilmer, C.B. Williams, M.J. Bortner, Current understanding and challenges in high temperature additive manufacturing of engineering thermoplastic polymers. Addit. Manuf. **34**, 101218 (2020). https://doi.org/10.1016/j.addma.2020.101218
16. S. Mohd Yusuf, S. Cutler, N. Gao, Review: the impact of metal additive manufacturing on the aerospace industry. Metals **9**, 1286 (2019). https://doi.org/10.3390/met9121286
17. E.A. Slejko, A. Gregorio, V. Lughi, Material selection for a CubeSat structural bus complying with debris mitigation. Adv. Sp. Res. **67**, 1468–1476 (2021). https://doi.org/10.1016/j.asr.2020.11.037
18. C. Casavola, A. Cazzato, V. Moramarco, G. Pappalettera, Influence of printing constraints on residual stresses of FDM parts, in: *Conf. Proc. Soc. Exp. Mech. Ser.*, 2018, pp. 121–127. https://doi.org/10.1007/978-3-319-62899-8_18.
19. M.A. Nazan, F.R. Ramli, M.R. Alkahari, M.A. Abdullah, M.N. Sudin, An exploration of polymer adhesion on 3D printer bed. IOP Conf. Ser. Mater. Sci. Eng. (2017). https://doi.org/10.1088/1757-899X/210/1/012062
20. M. Spoerk, J. Gonzalez-Gutierrez, C. Lichal, H. Cajner, G.R. Berger, S. Schuschnigg, L. Cardon, C. Holzer, Optimisation of the adhesion of polypropylene-based materials during extrusion-based additive manufacturing. Polymers (2018). https://doi.org/10.3390/polym10050490
21. O.S. Carneiro, A.F. Silva, R. Gomes, Fused deposition modeling with polypropylene. Mater. Des. **83**, 768–776 (2015). https://doi.org/10.1016/j.matdes.2015.06.053
22. M. Mohammadi, H. Fazli, M. Karevan, J. Davoodi, The glass transition temperature of PMMA: a molecular dynamics study

and comparison of various determination methods. Eur. Polym. J. **91**, 121–133 (2017). https://doi.org/10.1016/j.eurpolymj.2017.03.056

23. G. Palm, R.B. Dupaix, J. Castro, Large strain mechanical behavior of poly (methyl methacrylate) (PMMA) near the glass transition temperature. J. Eng. Mater. Technol. Trans. ASME. **128**, 559–563 (2006). https://doi.org/10.1115/1.2345447
24. D. Mathiesen, D. Vogtmann, R.B. Dupaix, Characterization and constitutive modeling of stress-relaxation behavior of Poly(methyl methacrylate) (PMMA) across the glass transition temperature. Mech. Mater. **71**, 74–84 (2014). https://doi.org/10.1016/j.mechmat.2014.01.003
25. R.B. Dupaix, M.C. Boyce, Constitutive modeling of the finite strain behavior of amorphous polymers in and above the glass transition. Mech. Mater. **39**, 39–52 (2007). https://doi.org/10.1016/j.mechmat.2006.02.006
26. D. Ahn, K.R. Shull, Effects of substrate modification on the interfacial adhesion of acrylic elastomers. Langmuir **14**, 3646–3654 (1998). https://doi.org/10.1021/la9713964
27. M. Spoerk, J. Gonzalez-Gutierrez, J. Sapkota, S. Schuschnigg, C. Holzer, Effect of the printing bed temperature on the adhesion of parts produced by fused filament fabrication. Plast. Rubber Compos. **47**, 17–24 (2018). https://doi.org/10.1080/14658011.2017.1399531
28. J. Zhang, X.Z. Wang, W.W. Yu, Y.H. Deng, Numerical investigation of the influence of process conditions on the temperature variation in fused deposition modeling. Mater. Des. **130**, 59–68 (2017). https://doi.org/10.1016/j.matdes.2017.05.040
29. N.G. Tanikella, B. Wittbrodt, J.M. Pearce, Tensile strength of commercial polymer materials for fused filament fabrication 3D printing. Addit. Manuf. **15**, 40–47 (2017). https://doi.org/10.1016/j.addma.2017.03.005
30. M.F. Afrose, S.H. Masood, P. Iovenitti, M. Nikzad, I. Sbarski, Effects of part build orientations on fatigue behaviour of FDM-processed PLA material. Prog. Addit. Manuf. **1**, 21–28 (2016). https://doi.org/10.1007/s40964-015-0002-3
31. T.M. Mower, M.J. Long, Mechanical behavior of additive manufactured, powder-bed laser-fused materials. Mater. Sci. Eng. A **651**, 198–213 (2016). https://doi.org/10.1016/j.msea.2015.10.068
32. D. Popescu, A. Zapciu, C. Amza, F. Baciu, R. Marinescu, FDM process parameters influence over the mechanical properties of polymer specimens: a review. Polym. Test. **69**, 157–166 (2018). https://doi.org/10.1016/j.polymertesting.2018.05.020
33. D.Y. Perera, Physical ageing of organic coatings. Prog. Org. Coat. **47**, 61–76 (2003). https://doi.org/10.1016/S0300-9440(03)00037-7
34. S. Lüftl, V.P.M., S. Chandran, eds., *Polyoxymethylene Handbook* (Wiley, Hoboken, 2014). https://doi.org/10.1002/9781118914458.
35. P. Hu, T. Shang, M. Jiang, M. Chen, Investigation of the thermal decomposition properties of polyoxymethylene. J. Wuhan Univ. Technol. Mater. Sci. Ed. **22**, 171–173 (2007). https://doi.org/10.1007/s11595-005-1171-6
36. B. Fayolle, J. Verdu, D. Piccoz, A. Dahoun, J.M. Hiver, C. G'sell, Thermooxidative aging of polyoxymethylene, part 2: embrittlement mechanisms. J. Appl. Polym. Sci. **111**, 469–475 (2009). https://doi.org/10.1002/app.29126
37. B. Fayolle, J. Verdu, M. Bastard, D. Piccoz, Thermooxidative ageing of polyoxymethylene, part 1: chemical aspects. J. Appl. Polym. Sci. **107**, 1783–1792 (2008). https://doi.org/10.1002/app.26648
38. J.M. Hutchinson, Physical aging of polymers, in *Prog. Polym. Sci.* (Springer, Dordrecht, 1995), pp. 703–760. https://doi.org/10.1016/0079-6700(94)00001-I
39. M. Celina, E. Linde, D. Brunson, A. Quintana, N. Giron, Overview of accelerated aging and polymer degradation kinetics for combined radiation-thermal environments. Polym. Degrad. Stab. **166**, 353–378 (2019). https://doi.org/10.1016/j.polymdegradstab.2019.06.007
40. Y. Shu, L. Ye, T. Yang, Study on the long-term thermal-oxidative aging behavior of polyamide 6. J. Appl. Polym. Sci. **110**, 945–957 (2008). https://doi.org/10.1002/app.28647
41. K. Tashiro, Molecular dynamics calculation to clarify the relationship between structure and mechanical properties of polymer crystals: the case of orthorhombic polyethylene. Comput. Theor. Polym. Sci. **11**, 357–374 (2001). https://doi.org/10.1016/S1089-3156(01)00005-8
42. B. Fayolle, E. Richaud, X. Colin, J. Verdu, Review: degradation-induced embrittlement in semi-crystalline polymers having their amorphous phase in rubbery state. J. Mater. Sci. **43**, 6999–7012 (2008). https://doi.org/10.1007/s10853-008-3005-3
43. A.S.D. Shackleford, R.J. Williams, R. Brown, J.R. Wingham, C. Majewski, Degradation of laser sintered polyamide 12 parts due to accelerated exposure to ultraviolet radiation. Addit. Manuf. (2021). https://doi.org/10.1016/j.addma.2021.102132
44. M.S. Rahman, U. Shaislamov, J.K. Yang, J.K. Kim, Y.H. Yu, S. Choi, H.J. Lee, Effects of electron beam irradiation on tribological and physico-chemical properties of Polyoxymethylene copolymer (POM-C). Nucl. Instrum. Methods Phys. Res. B **387**, 54–62 (2016). https://doi.org/10.1016/j.nimb.2016.10.001
45. K. Król-Morkisz, E. Karaś, T.M. Majka, K. Pielichowski, K. Pielichowska, Thermal stabilization of polyoxymethylene by PEG-functionalized hydroxyapatite: examining the effects of reduced formaldehyde release and enhanced bioactivity. Adv. Polym. Technol. **2019**, 1–17 (2019). https://doi.org/10.1155/2019/9728637
46. Y. Li, T. Zhou, Z. Chen, J. Hui, L. Li, A. Zhang, Non-isothermal crystallization process of polyoxymethylene studied by two-dimensional correlation infrared spectroscopy. Polymer (Guildf). **52**, 2059–2069 (2011). https://doi.org/10.1016/j.polymer.2011.03.007
47. J.R.C. Dizon, A.H. Espera, Q. Chen, R.C. Advincula, Mechanical characterization of 3D-printed polymers. Addit. Manuf. **20**, 44–67 (2018). https://doi.org/10.1016/j.addma.2017.12.002
48. V.D. Sagias, K.I. Giannakopoulos, C. Stergiou, Mechanical properties of 3D printed polymer specimens. Procedia Struct. Integr. **10**, 85–90 (2018). https://doi.org/10.1016/j.prostr.2018.09.013